

Spin-polarized droplets in the unitary Fermi gas

Piotr Magierski,^{1,2,*} Buğra Tüzemen,^{1,†} and Gabriel Włazłowski^{1,2,‡}

¹*Faculty of Physics, Warsaw University of Technology, Ulica Koszykowa 75, 00-662 Warsaw, Poland*

²*Department of Physics, University of Washington, Seattle, Washington 98195-1560, USA*



(Received 2 November 2018; published 16 September 2019)

We demonstrate the existence of a type of spatially localized excitations in the unitary Fermi gas: spin-polarized droplets with a peculiar internal structure involving an abrupt change in the pairing phase at the surface of the droplet. It resembles the structure of the Josephson- π junction occurring when a slice of a ferromagnet is sandwiched between two superconductors. The stability of the impurity is enhanced by the mutual interplay between the polarization effects and the pairing field, resulting in an exceptionally long-lived state. The prospects for its realization in experiments are discussed.

DOI: [10.1103/PhysRevA.100.033613](https://doi.org/10.1103/PhysRevA.100.033613)

I. INTRODUCTION

The unitary Fermi gas (UFG), routinely realized in ultracold atomic gases, is a remarkable system possessing universal properties. One of its features is an exceptionally strong pairing which results in a pairing gap of the order of half the Fermi energy [1]. Such a strong pairing field makes it an appealing system for studies of pairing-related phenomena. In particular, spin-imbalanced systems offer the possibility to investigate superfluidity under time-reversal symmetry-breaking conditions. Due to the different radii of Fermi spheres for spin-up and spin-down fermions one expects the appearance of effects characteristic for the FFLO phase [2,3], Sarma phase [4–7], or interior gap phase [8]. Unfortunately in trapped inhomogeneous gases the excess of majority-spin particles is expelled towards the edges of the cloud, and the predicted effects of nonstandard pairing mechanisms appear close to the trap boundaries [9–11], which make them difficult to observe experimentally. However, the recent experimental realization of boxlike traps offers the possibility to investigate almost-homogeneous systems and, thus, may eventually help in the detection of these exotic phases [12].

In spin-imbalanced systems the behavior of the pairing field at the interface between the superfluid (paired atoms) and the normal (excess of spin majority atoms) component is similar to that at the superconductor (S)–ferromagnet (F) junction [13]. The issue which is of paramount importance in the case of ultracold atoms, however, and makes it qualitatively different from solid state physics, is the stability and dynamics of these structures. Namely, in ultracold atomic gas the stability is governed by the same interaction that is responsible for its pairing properties. This is quite a different situation than in the case of solid state structures, where the long-range Coulomb interaction between heavy ions governs

the stability of, e.g., the SF junction, and the pairing properties of electrons contribute to transport and thermal properties only. In this article we describe a novel type of long-lived structure in ultracold atomic gas which appears when spin polarization is induced locally by an external potential.

II. SPIN-POLARIZED DROPLETS

Let us consider an unpolarized and uniform UFG. When a time-dependent and spin-polarizing potential is applied within a certain region and it is strong enough, it locally breaks Cooper pairs [see Fig. 1(a)]. Namely, it creates a region where the pairing field is weaker (or even vanishes) and is characterized by a nonzero spin imbalance $p(\mathbf{r}) = \frac{n_{\uparrow}(\mathbf{r}) - n_{\downarrow}(\mathbf{r})}{n_{\uparrow}(\mathbf{r}) + n_{\downarrow}(\mathbf{r})}$, where $n_{\uparrow(\downarrow)}$ is the density of spin-up (spin-down) fermions. Consequently due to the different locations of Fermi surfaces of spin-up and spin-down fermions, induced by the polarization, the pairing field starts to oscillate and changes sign inside the impurity. A similar situation is encountered at SFS junctions [13,14]. In Fig. 1(b) we present a sketch of the behavior of the order parameter Δ through the SFS junction within a thin ferromagnet layer. Regions close to the nodal points, where $\Delta \rightarrow 0$, store the unpaired particles [15], and in these regions the spin polarization is enhanced. This effect may be viewed also as a consequence of the occupation of certain Andreev states which are localized around the pairing nodal points due to the scattering of quasiparticles on a spatially varying pairing potential (see also Fig. 2). As a consequence the pairing nodal points and the enhanced spin-polarized regions are mutually connected. While the aforementioned effects are known it is surprising that the structure persists even if one removes the external potential. This self-sustained polarized droplet is presented in Fig. 1(c).

The natural question concerns the origin of the stability of the structure, which, as we argue in this paper, is particularly enhanced. If we ignore the pairing structure within the impurity, its stability is governed by the spin transfer processes which result from the scattering of quasiparticles on the interface between the superfluid and the spin-polarized region. If

*piotrm@uw.edu

†tuzemen@if.pw.edu.pl

‡gabriel.wlazlowski@pw.edu.pl

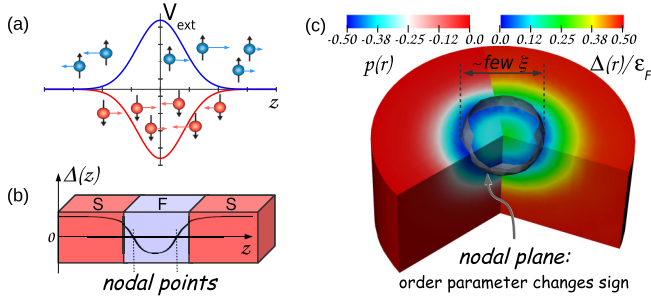


FIG. 1. (a) Spin-polarizing potential consisting of two Gaussian-shaped potentials that couple with different signs to different spin states. The potential generates a region where the system is locally polarized, $n_{\uparrow}(\mathbf{r}) \ll n_{\downarrow}(\mathbf{r})$. (b) Schematic structure of the order parameter Δ in the SFS junction, where the ferromagnet layer is sufficiently thin. Inside the layer the order parameter is suppressed and changes sign. (c) Structure of the polarized droplet. The spin polarization $p(\mathbf{r})$ and the pairing field $\Delta(\mathbf{r})$ distributions are shown on the left and right, respectively. The characteristic feature is the presence of the nodal surface of the pairing field at which the pairing changes its sign. The spin polarization reaches its maximum in the vicinity of the nodal surface.

the system is at low temperatures and not far from equilibrium the spin transfer, which in this regime is mainly due to Andreev reflection, is effectively suppressed [16–19]. However, the creation of the polarized impurity by the time-dependent potential brings the system relatively far from equilibrium. The process of inducing polarization creates various

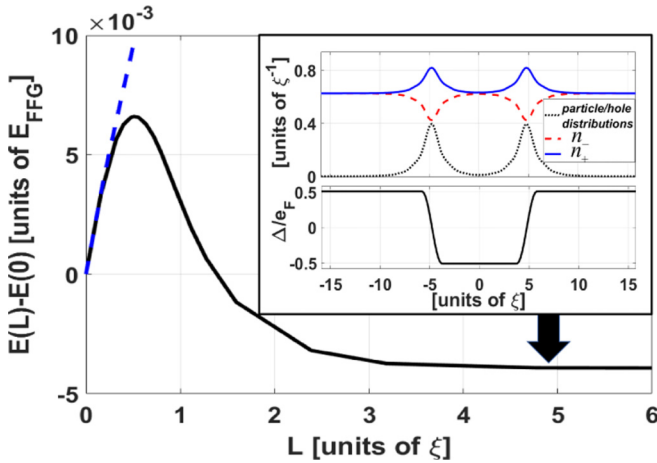


FIG. 2. Total energy of a 1D Fermi gas with (total) polarization $p = 0.05$ in an external pairing field as a function of the distance between pairing nodal points ($2L$). The dashed line indicates the energy of the configuration with the pairing set to 0 between nodal points. Inset: Pairing configuration (lower panel) at the distance indicated by the arrow; the upper panel shows the density distributions of spin-up and spin-down fermions and the particle (spin-up)/hole (spin-down) distributions associated with Andreev states localized around the nodal points, which are responsible for spin polarization. E_{FFG} denotes the energy of a uniform, unpolarized Fermi gas with the same number of particles; ξ is the coherence length of the corresponding uniform system.

phonon excitations in a superfluid, which would eventually decay into quasiparticle excitation and increase the temperature of the system. This effect would speed up the spin transfer processes between the polarized region and the surrounding superfluid, eventually leading to the disappearance of the impurity. When pairing is present inside the impurity the proximity effects, similar to those at the SFS junction, enhance the stability of the configuration. In order to understand better the reason for the stability it is instructive to consider the one-dimensional (1D) case. In this case the initially created structure starts to expand as the two polarized regions, in the vicinity of nodal points, repel each other. This in turn implies that the pairing field becomes complex, $\Delta \rightarrow \Delta \exp(iqx)$, and induces the current $|\vec{j}| \propto q$. As a result one ends up with two polarized regions which travel at finite velocity in opposite directions and the region between them becomes again fully paired (see Fig. 2). For more details of 1D calculations see Appendix C. In the 3D case this process, however, will not occur, as the radial expansion of the polarized region would inevitably increase the size of the polarized shell, which clearly costs energy. Thus the “surface tension” associated with the polarized shell counterbalances the repulsion and stabilizes the size of the impurity. Namely, the stability of the polarized impurity is dictated by the energy balance of the impurity energy, which can roughly be decomposed into two terms,

$$E_{\text{imp}} = E_{\text{shell}} + E_{\text{int}}, \quad (1)$$

where E_{shell} describes the energy of the polarized shell surrounding the impurity (concentrated around the pairing nodal surface) and E_{int} is the energy related to the impurity volume. The interplay between these terms leads to an enhanced stability in three dimensions. Similarly, the opposite process, leading to the collapse of the impurity, is suppressed due to the presence of the pairing field inside with an opposite phase. It creates an effective potential barrier, as the pairing inside has to be destroyed during the collapse. We emphasize that this configuration corresponds to an excited state. We dub it a ferron, since the pairing fields inside the impurity and at the SFS junction share many similarities.

The considerations concerning the stability of the polarized region allow for estimations of the minimum impurity size. It is clear that the pairing within the impurity needs a space to develop which is of the order of the BCS coherence length ξ . This sets the minimal limit for the size of the impurity to be stable. Numerical simulations show that the minimal radius of the stable ferron is about 2.5ξ .

III. NUMERICAL SIMULATIONS

A. Framework

In order to investigate the effect described above unconstrained 3D numerical calculations have been performed, using the framework based on time-dependent density functional theory in the form of the asymmetric superfluid local density approximation (TDSLDA). It allows for accurate treatment of the pairing correlations in a time-dependent fashion. It employs a density functional of generic form (we

set units to $m = \hbar = k_B = 1$) [20]:

$$\begin{aligned} \mathcal{E}_{\text{ASLDA}} = & \alpha_{\uparrow}(p) \frac{\tau_{\uparrow}}{2} + \alpha_{\downarrow}(p) \frac{\tau_{\downarrow}}{2} + \beta(p)(n_{\uparrow} + n_{\downarrow})^{5/3} \\ & + \frac{\gamma(p)}{(n_{\uparrow} + n_{\downarrow})^{1/3}} v^{\dagger} v + \sum_{i=\uparrow,\downarrow} [1 - \alpha_i(p)] \frac{\mathbf{j}_i^2}{2n_i}. \end{aligned} \quad (2)$$

The terms n_i , τ_i , v , and \mathbf{j}_i , respectively, denote the normal, kinetic, anomalous, and particle current densities, which are defined in terms of Bogoliubov quasiparticle wave functions $\{v_{n,i}, u_{n,i}\}$,

$$n_i(\mathbf{r}) = \sum_{|E_n| < E_c} |v_{n,i}(\mathbf{r})|^2 f_{\beta}(-E_n), \quad (3)$$

$$\tau_i(\mathbf{r}) = \sum_{|E_n| < E_c} |\nabla v_{n,i}(\mathbf{r})|^2 f_{\beta}(-E_n), \quad (4)$$

$$v(\mathbf{r}) = \sum_{|E_n| < E_c} v_{n,\downarrow}^*(\mathbf{r}) u_{n,\uparrow}(\mathbf{r}) \frac{f_{\beta}(-E_n) - f_{\beta}(E_n)}{2}, \quad (5)$$

$$\mathbf{j}_i(\mathbf{r}) = \sum_{|E_n| < E_c} \text{Im}[v_{n,i}(\mathbf{r}) \nabla v_{n,i}^*(\mathbf{r})] f_{\beta}(-E_n), \quad (6)$$

where E_n is the quasiparticle energy and E_c is the energy cutoff value as required by the regularization scheme. The Fermi-Dirac distribution, $f_{\beta}(E) = 1/(\exp(\beta E) + 1)$, where $\beta = 1/T$, allows us to model finite-temperature effects. The terms in the functional given by Eq. (2) have the following meaning: the first two describe the kinetic energies of particles with spin $i = \{\uparrow, \downarrow\}$ possessing effective masses α_i , and the third and fourth terms describe normal and pairing interactions, respectively, where strengths are controlled by the coefficients β and γ . The latter two terms are required in order to preserve the Galilean invariance of the theory. All coupling constants α_i , β , and γ are functions of the local polarization of the gas $p = \frac{n_{\uparrow} - n_{\downarrow}}{n_{\uparrow} + n_{\downarrow}}$. They have been adjusted to quantum Monte Carlo results for spin-imbalanced, homogeneous unitary Fermi gas and exhibit a remarkable agreement with the calculations for trapped systems [20,21]. In this way the density functional treatment offers a description of superfluidity beyond the mean-field Bogolubov–de Gennes (BdG) approximation, which is unable to reproduce correctly the quantum Monte Carlo data.

The TDASLDA equations can be obtained from the stationarity condition of the action,

$$S = \int_{t_0}^{t_1} \left(\langle 0(t) | i \frac{d}{dt} | 0(t) \rangle - E(t) \right) dt, \quad (7)$$

where $|0(t)\rangle$ denotes the quasiparticle vacuum at time t and $E(t)$ is the total energy

$$E(t) = \int \left(\mathcal{E}_{\text{ASLDA}}(\mathbf{r}, t) + \sum_{i=\uparrow,\downarrow} V_i(\mathbf{r}, t) n_i(\mathbf{r}, t) \right) d\mathbf{r}. \quad (8)$$

V_i is an arbitrary external one-body potential, which couples to the number density n_i . Formally TDASLDA equations resemble time-dependent Bogoliubov–de Gennes (TDBdG)

equations:

$$i \frac{\partial}{\partial t} \begin{pmatrix} u_{n,\uparrow}(\mathbf{r}, t) \\ v_{n,\downarrow}(\mathbf{r}, t) \end{pmatrix} = \begin{pmatrix} h_{\uparrow}(\mathbf{r}, t) & \Delta(\mathbf{r}, t) \\ \Delta^*(\mathbf{r}, t) & -h_{\downarrow}(\mathbf{r}, t) \end{pmatrix} \begin{pmatrix} u_{n,\uparrow}(\mathbf{r}, t) \\ v_{n,\downarrow}(\mathbf{r}, t) \end{pmatrix}. \quad (9)$$

Here $h_i(\mathbf{r}, t)$ denotes the single-particle Hamiltonian, which consists of kinetic, mean-field, and external potential terms. The pairing field Δ is proportional to the anomalous density v . Spin-reversed components of quasiparticle wave functions can be obtained via the symmetry relation $u_{n,\uparrow} \rightarrow v_{n,\uparrow}^*$, $v_{n,\downarrow} \rightarrow u_{n,\downarrow}^*$, and $E_n \rightarrow -E_n$.

The framework has been extensively tested over the last years, and it has proved to provide an accurate description of various dynamical properties of the strongly interacting Fermi gas, including generation and proliferation of quantum vortices [22] and dynamics of solitonic cascades [15,23]. More details related to technical aspects of solving TDASLDA equations are provided in Appendix A.

B. Demonstration of dropletlike properties of the ferron

The initial condition for simulations consists of a uniform solution of unpolarized UFG, at a very low temperature, $T/\varepsilon_F = 0.01$, where ε_F denotes the Fermi energy. In order to check the stability of the results with respect to finite-size effects, we used lattice sizes ranging from 40^3 to 64^3 . The lattice constant dx is chosen to be about three times smaller than the average interparticle distance $n^{-1/3}$, and the number of particles is fixed to get $k_F dx \approx 1$, where $k_F = (6\pi^2 n_{\uparrow})^{2/3}$ is the Fermi wave vector. Subsequently an external potential in the form of the Gaussian $V_i(\mathbf{r}, t) = \lambda_i A(t) e^{-r^2/2\sigma^2}$ of width σ and amplitude $A_0 = \max[A(t)]$ has been applied. The potential is spin dependent, attracting spin-down atoms ($\lambda_{\downarrow} = -1$) and repelling spin-up atoms ($\lambda_{\uparrow} = 1$), as shown in Fig. 1(a). The potential is switched on for a time interval sufficient to induce spin polarization locally, leading to the destruction of Cooper pairs within the region of radius $R \approx \sigma$. Eventually the external potential is removed, and the system evolves in time. For more details on the protocol for the impurity generation see Appendix B. In Fig. 3 the time evolution of the local polarization, induced at the center of the simulation box $p(\mathbf{r} = 0)$, is presented. In Fig. 3(b) the relative phase of the pairing field at the center of the polarized region, measured with respect to the phase outside the impurity $\Delta\varphi = \varphi_{\text{in}} - \varphi_{\text{out}}$, is shown, where $\varphi = \arg \Delta$. Simulations were performed for the external potential of the amplitude $A_0 = 2\varepsilon_F = k_F^2$ and three widths, $\sigma/\xi = 2.38, 3.14,$ and 7.07 . The potential has been applied within the time interval $t < 150\varepsilon_F^{-1}$. In the first two cases the time interval was sufficiently long to generate a region of high local polarization $p \gtrsim 0.8$ with an almost-vanishing pairing field $\Delta(\mathbf{r}) \approx 0$ inside the region. The evolution after the potential was removed turned out to be different and depended crucially on the size of the polarized region. A too small polarization radius $\sigma \lesssim 3\xi$ does not provide enough space to develop the aforementioned oscillatory pairing field pattern. As a result it is not stabilized by the pairing field and decays. For larger sizes, $\sigma \gtrsim 3\xi$, as the potential is removed, the pairing field inside the impurity reappears with the opposite phase. Moreover, within the time scale $1000\varepsilon_F^{-1}$ there is no visible decrease in the polarization,

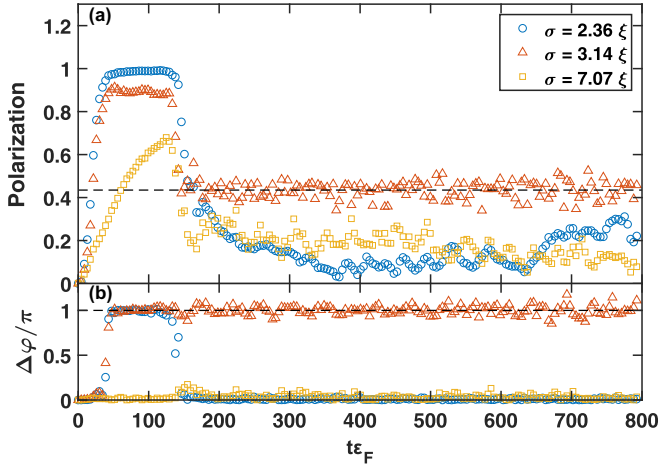


FIG. 3. Time evolution of the local polarization $p(\mathbf{r} = 0)$ in the center of the box (a) and the pairing phase difference $\Delta\varphi$ (b). An external potential of strength $A_0 = 2\varepsilon_F$ and various widths σ has been applied within the time interval $0-150\varepsilon_F^{-1}$. In the case where $\sigma = 3.14\xi$ stabilization of the polarization and the phase difference at a constant value for $t\varepsilon_F > 150$ indicates creation of the ferron. For animations showing the distributions of both the local polarization $p(\mathbf{r})$ and the pairing field $\Delta(\mathbf{r})$ see the movies in the Supplemental Material [24].

indicating the unusual stability of the polarized droplet. In the latter case, for $\sigma \approx 7\xi$, the potential acts within a time interval too short to excite the ferron. Thus, both the potential radius and its duration have to be large enough to generate the stable polarized droplet. It turns out that in the latter scenario the time interval needs to be increased by at least a factor of 2 in order to produce a self-sustained spin-polarized droplet.

The numerical simulations indicate that there is a preferable shape and size of the impurity. The calculations reveal that changing the potential width σ within the range $3\xi-7\xi$ weakly affects the size of the generated ferron. In each case the measured radius of the droplet (defined as the distance to the nodal surface) evolves towards a value within the interval $2.5\xi-3.5\xi$. Another dropletlike feature of the ferron can be observed when a deformed impurity is generated. Namely, the external potential in the form of a Gaussian function $V_i = \lambda_i A \exp(-\frac{x^2}{2\sigma_x^2} - \frac{y^2}{2\sigma_y^2} - \frac{z^2}{2\sigma_z^2})$ with different widths $\sigma_{x,y,z}$ in each spatial direction induces initially a deformed impurity. However, it evolves rather rapidly (within a time of order $100\varepsilon_F^{-1}$) towards an almost spherically symmetric configuration. These results confirm that the peculiar pairing structure is responsible for the existence and stability of the ferron. The spherical shape of the droplet at a fixed volume minimizes E_{shell} , without affecting E_{int} , whereas the preferable size of the impurity is due to the nodal structure of the pairing field.

The above simulations demonstrate that ferrons in 3D form long-lived excitations and indeed bear similarities to droplets. In order to investigate this aspect further the collisions of two initially separated ferrons have been performed. They have been generated by applying two spin-selective potentials moving towards each other. The potentials' velocities, generating ferrons, were set lower than the speed of sound and the process of head-on collision is shown in Fig. 4. Note that the structure of ferrons is preserved during the collisions. They fuse and

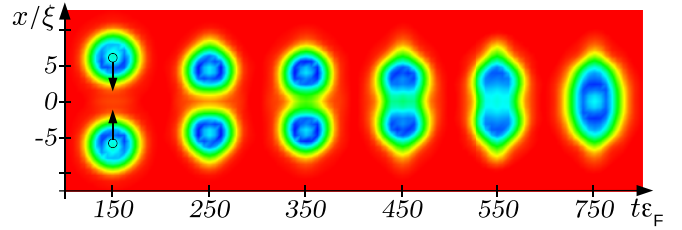


FIG. 4. Head-on collision of two ferrons. The droplets were created by two moving potentials of amplitude $A = 2\varepsilon_F$ and width $\sigma = 3.14\xi$ as indicated by the arrows. The potentials were applied within the time interval $0-150\varepsilon_F^{-1}$, and snapshots of the pairing field spatial distributions $\Delta(\mathbf{r})/\varepsilon_F$ taken at later times (as indicated by labels on the horizontal axis). Color coding is the same as in Fig. 1. For a full movie see the Supplemental Material [24].

a new droplet of a larger size is created with the typical pairing nodal structure. Although initially the obtained ferron is deformed one expects that it will evolve toward a spherical shape, which may take a relatively long time, as it is immersed in an excited superfluid bath.

Finally, we have also checked that qualitatively the same results are obtained within the mean-field BdG approach; see Appendix D for comparison. This means that the existence of the stable ferron is not sensitive to the choice of a particular form of the functional.

IV. STABILITY OF THE RESULTS WITH RESPECT TO PERTURBATIONS

A. The impurity stability vs its size

The width σ of the external spin-polarizing potential, Eq. (B1), represents an important parameter in the process of droplet generation. If it is too small, then inside the polarized region there is not enough space to allow for the order parameter fluctuations, which naturally occur at the scale of the coherence length (ξ). Therefore, based on the presented argument, one expects that σ has to be at least of the order of ξ . Numerically we have confirmed that the minimal width needed for successful creation of the ferron is indeed $\sigma \gtrsim 3\xi$, which is a threshold value (as we go through the impurity the phase difference varies from 0 to π and again to 0). In Fig. 5 we present the time evolution of the spin polarization inside the impurity and the phase difference between the interior and the outside regions, for different values of σ . It is clearly shown that for widths exceeding the coherence length ξ by a factor of 3, both the polarization and the phase difference remain fairly constant during the simulations, which correspond to times $t\varepsilon_F \approx 1000$. Note that as we increase the width of the potential we excite more phonons in the background superfluid. These fluctuations propagate towards the edges of the box, and due to periodic boundary conditions they again reenter the box and interfere with the ferron structure. This effect, which is due to the finite size of the box and imposed periodic boundary conditions, gives rise to oscillations of the phase difference, especially visible for the case with $\sigma = 6.28\xi$.

Performed calculations indicate the existence of a preferable size of the impurity. In order to demonstrate this feature,

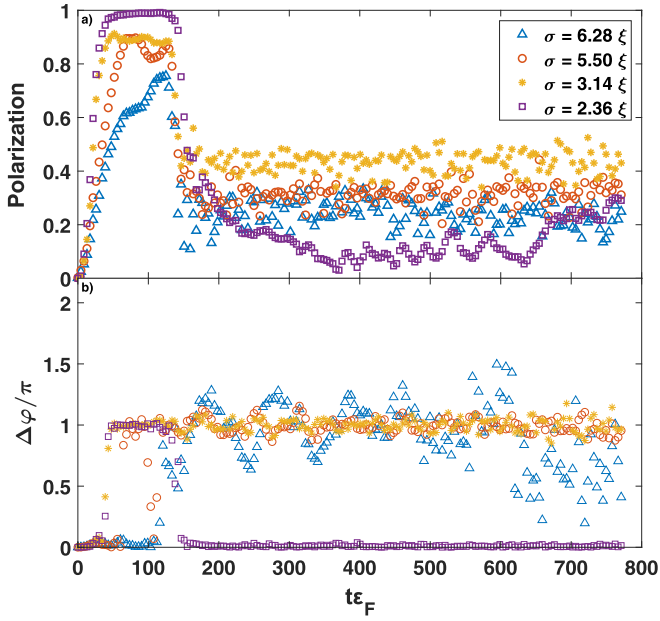


FIG. 5. Impact of the spin-polarizing potential width σ on the process of impurity generation. (a) Time evolution of the local polarization in the center of the impurity; (b) pairing phase difference. The box size, 40^3 , corresponds to a length of 31ξ along each dimension. The amplitude of the potential was fixed at $A_0 = 2 \epsilon_F$. Results for $\sigma \gtrsim 3 \xi$ correspond to the cases where a ferron was successfully created. Calculations presented in this graph are shown in Supplemental Movies 1–4 [24].

let us consider a certain volume V_π characterized by the shifted phase (by π) of the order parameter with respect to the value far away from the polarized region. This volume may serve to define the radius of the ferron by means of the relation $V_\pi = \frac{4}{3}\pi r^3$. In Fig. 6 we present the radii of impurities, generated by potentials of different widths σ , as a function of the time. It is clearly visible that increasing the width of the spin-polarizing potential above the value $\sigma \gtrsim 4 \xi$ does not lead to the creation of impurities with larger radii. Instead it is observed that in most cases the size of the impurity remains essentially constant at $r \approx 3.5 \xi$.

B. The impurity stability vs the potential strength

We have analyzed the impact of the potential strength A_0 on the process of impurity formation. The time evolution of the spin polarization inside the impurity and the phase difference for three selected strengths are presented in Fig. 7.

If the amplitude is too low, $A_0 \lesssim \epsilon_F$, then the potential is too weak to break efficiently Cooper pairs and to induce locally a sufficiently large spin polarization. As a consequence a stable impurity is not formed. On the other hand, if the amplitude is too high, $A_0 \gtrsim 4 \epsilon_F$, the potential induces excitations of the background superfluid (e.g., phonon excitations) which have sufficient energy to effectively interfere with the ferron structure, leading to its decay. Thus there is a particular range of potential amplitudes for which we observe the creation of a long-lived impurity.

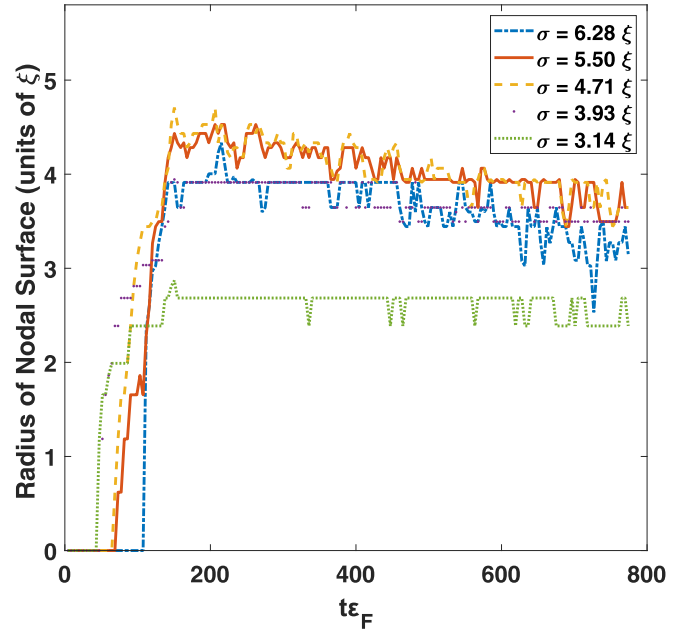


FIG. 6. Time evolution of radii of impurities generated by potentials of different widths σ . The amplitude of the potential was fixed at $A_0 = 2 \epsilon_F$. The potential was turned off at time $t_{\text{off}} = 150 \epsilon_F^{-1}$. Variations of radii at short time scales are related to the finite resolution of the lattice.

C. Deformed impurities

In most of the simulations, we used the spin-polarizing potential, (B1), with additional, small symmetry-breaking

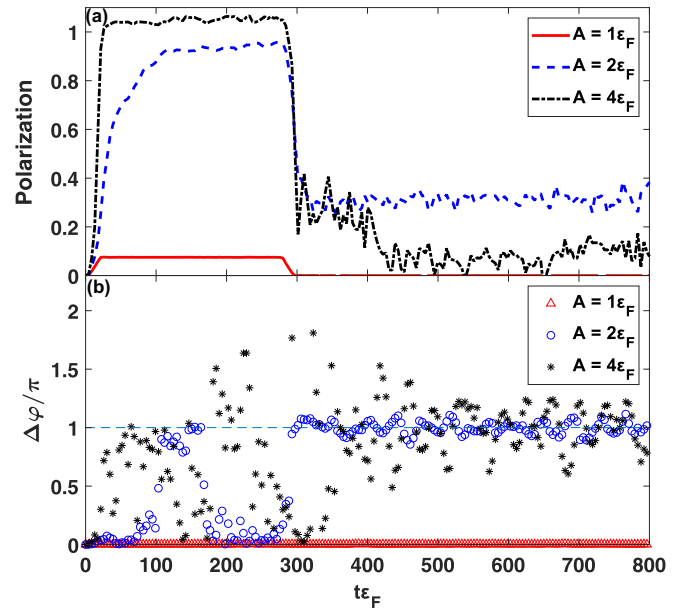


FIG. 7. Time evolution of the central local spin polarization (a) and pairing phase difference (b) for impurities generated by potentials of different strengths. The simulation box is 48^3 , which corresponds to 38ξ along in each dimension. The width of the Gaussian potential is set to $\sigma = 4.71$. For the three presented scenarios, only the potential of strength $A_0 = 2 \epsilon_F$ produces a stable ferron.

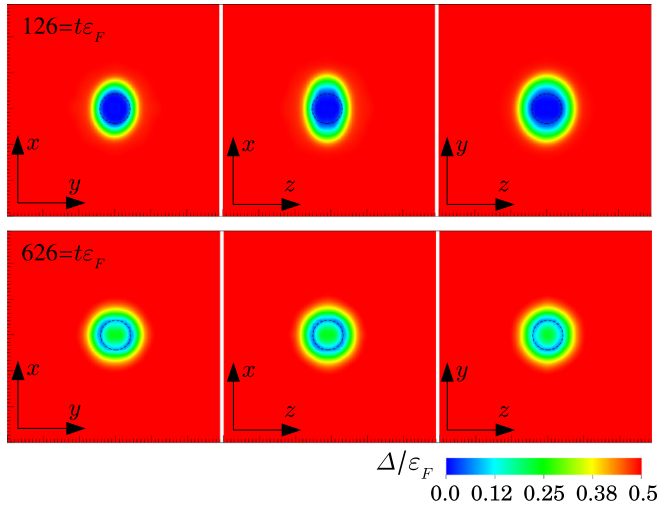


FIG. 8. Cross sections through the pairing field $\Delta(\mathbf{r})$ along three perpendicular planes. The top row shows the pairing field configurations just before the deformed potential ($\sigma = 4.7\xi$, $\epsilon_y = 0.44$, and $\epsilon_z = 0.64$) is switched off. The bottom row shows the pairing field configurations after the potential is switched off and the system has evolved for an additional time interval $500 \epsilon_F^{-1}$. The plot indicates that a spherical shape is the preferable configuration for a ferron. For a full video see Supplemental Movie 8 [24].

parameters $|\epsilon_{y/z}| \approx 10^{-6}$. In this case, almost spherically symmetric impurities were created. In order to explore the possibility of creation of a deformed impurity and to investigate its stability, we have executed runs involving a strongly deformed external potential. Namely, we set potential parameters: $\epsilon_y = 0.44$ and $\epsilon_z = 0.64$. We have found that the generated impurity is as stable as the one generated by a nearly spherically symmetric potential. Moreover, the potential generated initially deformed the impurity, which subsequently evolved toward a spherical configuration (see Fig. 8). This demonstrates that the spherical shape represents the most favorable configuration.

D. Collision of impurities

Since ferrons are long-lived and localized excitations, one may consider scenarios which are sensitive to their mutual arrangements and investigate their dynamics involving collisions. There are several issues which may be explored and here we touch upon only the most basic ones. Namely, there is clearly an induced interaction between ferrons which is mediated by the superfluid background. The natural question is how strong this interaction is and whether it may effectively repel or attract impurities. The second question is whether the peculiar structure of the ferron is rigid enough to survive collision or whether collision leads to its immediate decay. As examples of such scenarios, we performed simulations where we collided two ferrons. The ferrons were created by means of two moving potentials along the x axis. The velocity of potentials was set lower than the speed of sound. The shape of each potential was determined by Eq. (B1). In Fig. 9 we show a few snapshots of a collision with a nonzero impact parameter. We observe a fusion process which results in the

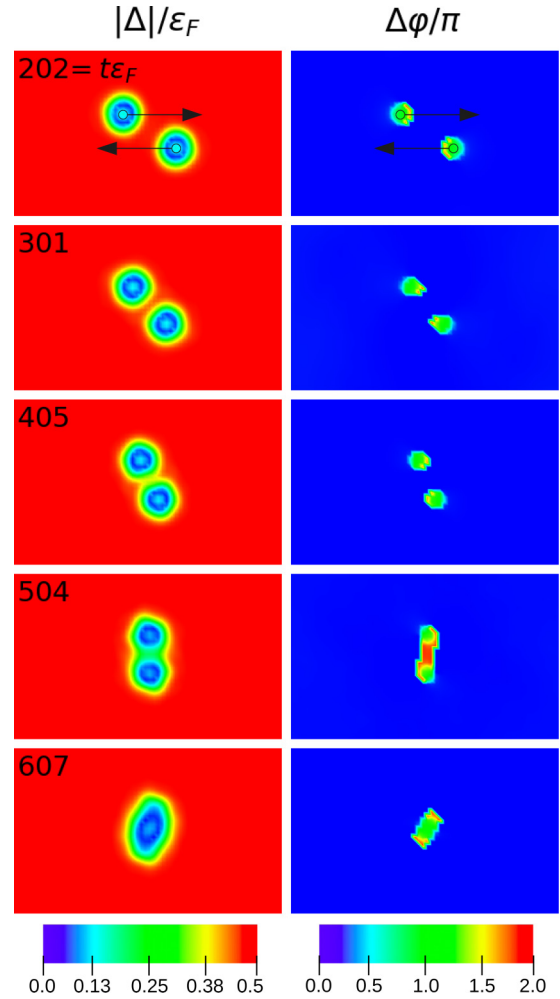


FIG. 9. Snapshots from a simulation demonstrating the peripheral collision of two ferrons. In the left column the absolute value of the pairing field is plotted; in the right column, the pairing phase difference (with respect to the value at the box edge). For the full video see Supplemental Movie 9 [24].

creation of a new stable ferron. These simulations indicate that the ferron states represent very stable configurations.

V. EXPERIMENTAL REALIZATION

Recent developments of experimental techniques allow us to implement spin-dependent potentials using close-to-resonance laser beams [25]. Both the size and the strength of the beam can be controlled. In order to induce ferron excitation it is not sufficient to polarize the system locally; the spin-polarizing potential has to be strong enough to allow the pairing field to reappear with the flipped phase. Clearly, the potential strength must be at least of the order of the pairing gap, which is quite large for a UFG, $\Delta/\epsilon_F \approx 0.5$. Our calculations indicate that a potential of amplitude $A_0 \approx \epsilon_F$ is not sufficient to induce a ferron, and one needs $A_0 \approx 2 \epsilon_F$ for efficient droplet creation. Therefore we suggest using two crossing laser beams, each of about ϵ_F amplitude. In the crossing region the amplitude will be enhanced to the required strength, allowing for the creation of a localized

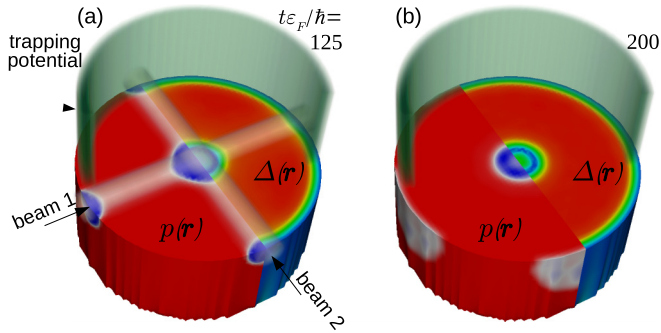


FIG. 10. Idea of an experimental protocol leading to ferron creation in a boxlike trap. Each panel shows the spatial distribution of the local polarization $p(\mathbf{r})$ and the pairing field $\Delta(\mathbf{r})$. Color coding is the same as in Fig. 1. Two crossing beams, each of amplitude $A_0 = 1 \varepsilon_F$ and width $\sigma = 3.14 \xi$, are applied for time $t \varepsilon_F / \hbar = 150$. (a) Only in the crossing region the total strength is sufficient to efficiently polarize the gas. (b) After removal of the beams, the polarized region converts into a stable ferron. For the full video see the Supplemental Movie 11 [24].

ferron. This procedure has been tested numerically for a UFG confined in a box trap [12] (see Fig. 10).

It must be emphasized that the associated time scales are also experimentally accessible. In the numerical tests, we applied the polarizing potential for time intervals of about $150 \varepsilon_F^{-1}$, and we concluded that the lifetime of ferrons is at least $1000 \varepsilon_F^{-1}$. Assuming the value of Fermi energy for a typical experimental setup $\varepsilon_F \approx h \times 13$ kHz according to Ref. [12], the required time for a beam impulse is 2 ms, which subsequently allows at least 12 ms for ferron detection, e.g., by measuring the density difference between two spin states.

The mechanism responsible for the stability of a ferron is generic and is valid on both the BEC and the BCS side. However, other features of the system come into play when one considers these limits. The energy needed to create a ferron scales approximately linearly with the pairing gap $E_{\text{imp}} \sim |\Delta|$, as the main energy cost comes from breaking of the Cooper pairs. On the BCS side, the condensation energy scales as $E_{\text{cond.}} \sim |\Delta|^2$, and thus these two scales will become comparable in the deep BCS regime. Therefore by trying to induce local spin imbalance (a ferron) in the system one may likely remove the pairing completely, turning the system into the normal phase. For more details, see Appendix C. In the opposite BEC limit two energy scales exist: one associated with the binding energy of composite bosons, which is steeply rising on the BEC side, and one related to the condensation temperature, which is fairly constant. In order to locally spin-polarize the BEC one needs to break up composite bosons, which requires rather strong laser beams, which would lead to extensive excitation. In our tests (see Sec. IV B), we find that even at unitarity the application of strong potentials (like $A_0 \gtrsim 4 \varepsilon_F$) typically induces too many phonons, which effectively interfere with the ferron structure, leading to its destruction. Thus, we predict that the unitary regime is the most suitable for ferron creation. There is also another technical problem, namely, close-to-resonance laser beams may heat up the system due to incoherent scattering

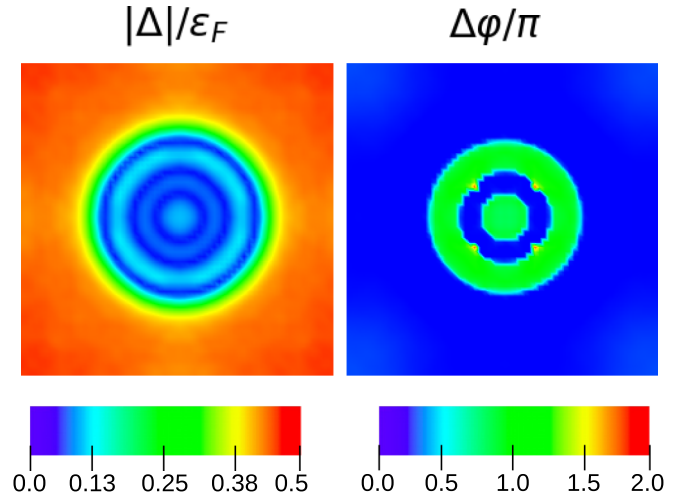


FIG. 11. Snapshot from a simulation demonstrating the internal structure of a large ferronlike excitation taken after time $\Delta t \approx 220 \varepsilon_F^{-1}$ with respect to the moment when the potential was removed. It is clearly shown that the phase changes sign three times as we proceed towards the center of the impurity. For the full video see Supplemental Movie 13 [24].

of photons (an effect not included in our simulations) and thus cause loss of superfluidity before the ferron structure is created. This aspect requires more sophisticated analysis which is beyond the scope of this work.

VI. IMPURITIES WITH A MORE COMPLEX INTERNAL STRUCTURE

Studies of proximity effects on SFS junctions proved that the order parameter may change sign a few times, depending on the width of the ferromagnet layer [13,14]. A similar effect is also expected in the case of ferronlike excitations. In order to investigate this possibility, we performed exploratory simulations using an external potential of a large width, $\sigma = 11.8 \xi$, and high amplitude, $A_0 = 3.5 \varepsilon_F$. Indeed, we have observed that after removal of the potential (at time $t_{\text{off}} \varepsilon_F \approx 170$) inside the impurity the order parameter changes signs a few times as we move towards the center. A sample configuration is presented in Fig. 11. The simulation revealed also that the internal pairing structure exhibits various oscillations in time. Further studies are required in order to determine whether these oscillations are related to the internal dynamics of the impurity or originate from the superfluid background fluctuations.

VII. CONCLUSIONS

We have demonstrated using state-of-the-art time-dependent density functional theory that one may create, in the bulk of a unitary Fermi gas, a surprisingly long-lived excitation consisting of a spin-polarized region characterized by a peculiar structure of the pairing field, which governs its stability. The mechanism responsible for its creation is similar to the one responsible for the FFLO phase or for the appearance of a Josephson- π junction in SFS structures.

The experimental conditions for creation of these structures (ferrons) are within reach and may offer the possibility to explore a plethora of new phenomena involving dynamics and interactions between ferrons and, e.g., quantum vortices or domain walls. Note also that their creation and detection may turn out to be simpler than the detection of the FFLO phase and thus would provide an indirect strong argument for the existence of this long-sought phase [26].

ACKNOWLEDGMENTS

We are grateful to A. Bulgac and G. Bertsch for discussions and critical remarks. This work was supported by the Polish National Science Center (NCN) under Contracts No. UMO-2016/23/B/ST2/01789 (P.M., B.T.) and No. UMO-2017/26/E/ST3/00428 (G.W.). We acknowledge PRACE for awarding us access to the resource Piz Daint based at the Swiss National Supercomputing Centre (CSCS), Decision No. 2017174125. We also acknowledge the Global Scientific Information and Computing Center, Tokyo Institute of Technology for resources at TSUBAME3.0 (Project ID hp180066), and Interdisciplinary Centre for Mathematical and Computational Modelling (ICM) of Warsaw University for computing resources at Okeanos (Grant No. GA67-14). The contribution of each of the authors was significant and the order of the names is alphabetical.

APPENDIX A: NUMERICAL IMPLEMENTATION OF THE TDASLDA

Calculations have been performed using the numerical code constructed for studies of solitonic cascades in a spin-imbalanced unitary Fermi gas (UFG). It was described in detail in the Supplemental Material to Ref. [15] and therefore here we limit the description to the most important details. The code solves TDASLDA equations [20] (which have the formal structure of time-dependent Bogoliubov–de Gennes equations) on a 3D spatial lattice without any symmetry restrictions. Periodic boundary conditions are imposed. Spatial derivatives appearing in the single-particle Hamiltonian are calculated using spectral methods (via FFTs), while for time integration the Adams-Bashforth-Moulton (predictor-corrector) scheme of fifth order is implemented. In order to accelerate computations, graphics processing units (GPUs) are utilized. In calculations presented here the number of GPUs exceeded 128 (nvidia P100) and in some cases (for large lattices) it reached 1600. Calculations were performed on the TSUBAME3.0 (Tokyo Institute of Technology) and Piz Daint (CSCS, Switzerland) supercomputers.

We have used lattice sizes ranging from 40^3 up to 64^3 , with lattice constant $dx = 1$. Various box volumes allowed us to investigate the influence of finite-size effects on the stability of ferrons. In each simulation the number of particles was chosen in such a way as to satisfy the condition $k_F = (6\pi^2 n_\uparrow)^{1/3} = 1$. In the case of the smallest box (40^3) this requirement corresponds to 1081 particles per single spin state. The integration time step Δt was taken to be $\Delta t = 0.005 \varepsilon_F^{-1}$ (units are set by the requirement $m = \hbar = 1$). This integration time step enabled us to execute numerically stable simulations within time intervals $t_{\max} \approx 1000 \varepsilon_F^{-1}$.

APPENDIX B: PROTOCOL FOR IMPURITY GENERATION

The initial condition for simulations consists of the uniform solution of an unpolarized UFG at a very low temperature, $T/\varepsilon_F = 0.01$. The self-consistent solution of ASLDA equations for a uniform system provided the correct system properties, namely, $E/E_{\text{FFG}} = 0.40(1)$ (Bertsch parameter) and $\Delta/\varepsilon_F = 0.50(1)$, where uncertainties arose due to finite-size effects, related to various lattice sizes used in the calculations. Having a uniform, unpolarized solution of the ASLDA, we subsequently applied a spin-selective external potential that locally polarized the system,

$$V_i(\mathbf{r}, t) = \lambda_i A(t) \exp \left[-\frac{x^2 + (1 - \epsilon_y)y^2 + (1 - \epsilon_z)z^2}{2\sigma^2} \right], \quad (\text{B1})$$

where $\lambda_\uparrow = +1$ denotes spin-up particles (repulsive potential) and $\lambda_\downarrow = -1$ denotes spin-down particles (attractive potential). The width of the Gaussian potential σ was set to be a few times larger than the BCS coherence length, $\xi \approx 1.27$. The coefficients $|\epsilon_{y/z}| \ll 1$ were introduced in order to break the spherical symmetry of the potential. The amplitude $A(t)$ varied in time according to the prescription

$$A(t) = \begin{cases} A_0 s(t, t_{\text{on}}), & 0 \leq t < t_{\text{on}}, \\ A_0, & t_{\text{on}} \leq t < t_{\text{hold}}, \\ A_0 [1 - s(t - t_{\text{hold}}, t_{\text{off}} - t_{\text{hold}})], & t_{\text{hold}} \leq t < t_{\text{off}}, \\ 0, & t \geq t_{\text{off}}, \end{cases} \quad (\text{B2})$$

where $s(t, w)$ denotes a function which smoothly varies from 0 to 1 within the time interval $[0, w]$:

$$s(t, w) = \frac{1}{2} + \frac{1}{2} \tanh \left[\tan \left(\frac{\pi t}{w} - \frac{\pi}{2} \right) \right]. \quad (\text{B3})$$

A_0 denotes the amplitude of the potential, which we typically set to be about $A_0 \approx 2 \varepsilon_F$. In Fig. 12 we present the typical energy evolution of a system that is the subject of an external spin-polarizing potential that is switched on at a certain rate and subsequently switched off. It is clearly shown that the

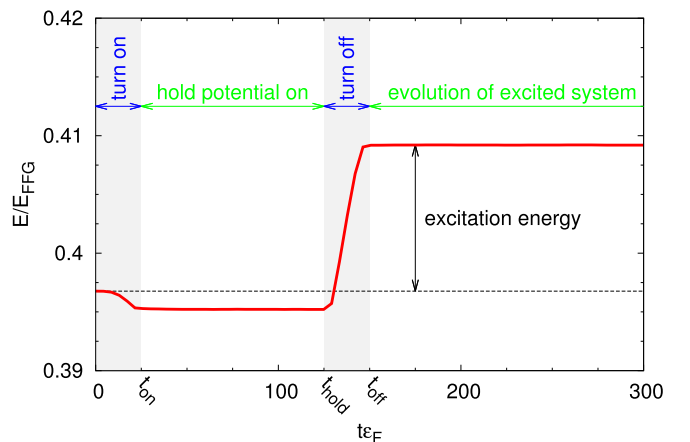


FIG. 12. Example of the time evolution of the total energy of the system.

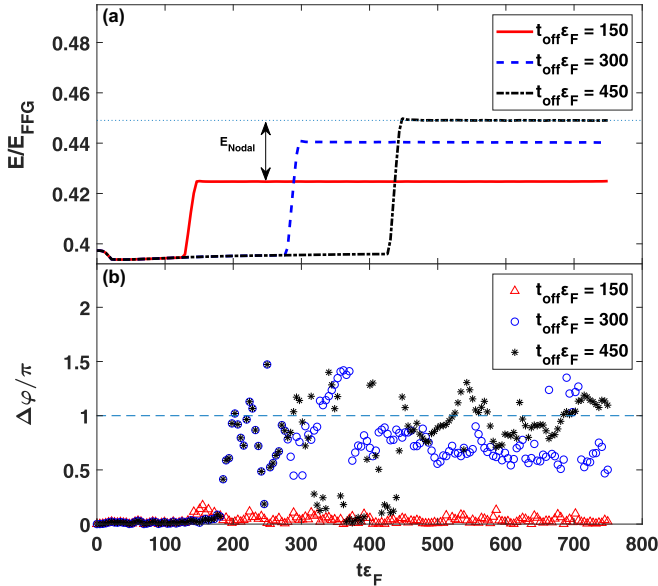


FIG. 13. Time evolution of the total energy (a) and pairing phase difference between the polarized region and the outside superfluid background (b). Presented results were obtained for three time intervals during which the external potential was turned on. In the first case (red triangles) the potential was applied within the time interval $t_{\text{off}} \varepsilon_F \approx 150$, whereas in the other cases the time interval was enlarged by a factor of 2 and 3, respectively. The amplitude of the potential is $A_0 = 2 \varepsilon_F$ and the width is $\sigma = 7.07 \xi$. Calculations presented in this figure are shown in Supplemental Movies 5–7 [24].

energy changes only within time intervals when the external potential V_i is turning on and off. Otherwise, the total energy of the system is conserved. The energy difference, $\Delta E = E(t_{\text{off}}) - E(0)$, can be attributed to the excitation energy of the system, and it roughly measures the energy contained in the impurity (one needs to remember that creation of the impurity in real time generates also various background oscillations, which carry part of the energy).

It is important to stress that the generation of a stable ferron requires some time. If the external potential is applied within a time interval that is too short, the system will not manage to develop a peculiar structure of the pairing field, with the phase shifted by π inside the polarized region. This situation is demonstrated in Fig. 13, where we have compared three types of calculations, differing by the time interval during which the potential was kept at its maximum strength. It is clearly shown that in the case of the potential which is completely turned off at $t_{\text{off}} \approx 150 \varepsilon_F^{-1}$, a phase difference between the interior of the polarized region and the outside superfluid is not created. In the second case, where the spin-selective potential was kept on twice as long, we observed that a certain phase difference developed. It does not reach the value of π , however, and the impurity decays. Finally, for the potential duration $t_{\text{off}} \varepsilon_F \approx 450$ we have observed that a phase difference π is developed. It results in the generation of a nodal surface, which strongly suppresses the effects responsible for the decay. The energy plot demonstrates that there is indeed a certain energy cost related to the generation of the nodal surface, which can be quantified as the total energy difference for states with versus

without the flipped phase. This contribution to the energy is depicted as E_{nodal} in Fig. 13.

APPENDIX C: INSTABILITY OF FERRONS IN ONE DIMENSION

We have argued that the stability of ferrons is attributed to their geometry and dimensionality. Here we present a simple example visualizing the instability of a ferron in one dimension. Namely, we have applied the TDBdG approach in one dimension (all quantities depend on the position x and time t , which we drop for notation brevity),

$$i \frac{\partial}{\partial t} \begin{pmatrix} u_{n,\lambda} \\ v_{n,-\lambda} \end{pmatrix} = \begin{pmatrix} h_\lambda & \lambda \Delta \\ \lambda \Delta^* & -h_{-\lambda}^* \end{pmatrix} \begin{pmatrix} u_{n,\lambda} \\ v_{n,-\lambda} \end{pmatrix}, \quad (\text{C1})$$

where $\lambda = \pm 1$ denotes spin indices, $h_\lambda(x, t) = -\frac{1}{2} \frac{d^2}{dx^2} + gn_{-\lambda}(x, t) + V_\lambda(x, t)$, and $\Delta(x, t) = gv(x, t)$ (n_λ is the density of spin- λ particles, v is the anomalous density). The coupling constant g has been adjusted so as to fulfill the condition $\Delta/\varepsilon_F \approx 0.5$, $\varepsilon_F = \frac{k_F^2}{2}$. In one dimension one may generate a similar form of spin-polarized impurity. Supplemental Movie 14 [24] shows an example of a ferron in one dimension created by the potential,

$$V_\lambda(x, t) = 1.8 f(t) \lambda \varepsilon_F \exp\left(-\frac{x^2}{2\sigma^2}\right), \quad (\text{C2})$$

where

$$f(t) = \sin^2\left(\frac{\pi t}{2T}\right) \theta(T_1 - t) + \theta(t - T_1) \theta(T_2 - t) + \cos^2\left(\frac{\pi(t - T_2)}{2T}\right) \theta(t - T_2) \theta(T_1 + T_2 - t) \quad (\text{C3})$$

describes the switching-on and switching-off rates. For the particular realization of the ferron shown in Supplemental Movie 14 we used the parameters $k_F \sigma = 4.441$, $T = T_1 = 29.55 \varepsilon_F^{-1}$, and $T_2 = 49.25 \varepsilon_F^{-1}$. Note that after the initial creation of a ferron with a characteristic structure of the pairing field, the polarized regions are repelled by each other and the system between them becomes again fully paired. This behavior, which can also be understood by means of the results presented in Fig. 2, indicates that the ferron is unstable in one dimension.

It is also instructive to analyze the structure of the ferron and its excitation energy as a function of the pairing gap. This sheds light on the properties of the ferron when moving from a unitary regime towards the BCS limit. We performed an analysis in one dimension using the BdG approach. Namely, we considered a spin-imbalanced system with $N + 2$ spin-up and $N - 2$ spin-down fermions on a lattice of size L with periodic boundary conditions. The spin imbalance generates two nodes of the pairing field, which we have placed at $x = \pm L/4$. This is the only possibility of generating a stationary configuration in one dimension. We have calculated the energy of such a configuration with respect to a uniform, unpolarized system of N spin-up and N spin-down fermions. The results are shown in Fig. 14 as a function of the pairing gap of the uniform system. It is clearly shown that the energy, which can be thought of as the excitation energy associated with the creation of the nodal structure of the

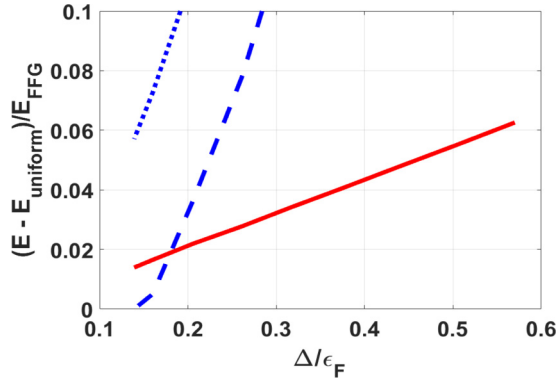


FIG. 14. The energy of the ferronic structure in one dimension (with respect to the uniform system) vs the pairing gap for $N = 20$ and $L = 200$ (see text for details) is indicated by the solid red line. The dashed blue line and dotted blue line show the pairing energies for the spin-imbalanced system: $N + 2$ spin-up fermions, $N - 2$ spin-down fermions and uniform, unpolarized system, respectively.

pairing field in the spin-imbalanced system, changes linearly with the magnitude of the pairing gap. This is because the main energy cost comes from local spin polarization of the system, i.e., breaking of Cooper pairs. The size of the ferron is much larger in the weak-coupling limit due to the increase in the coherence length, which makes the polarized shell surrounding the ferron significantly wider than in the unitary regime. The dashed lines shown in the figure indicate the behavior of the condensation energy, which scales as $E_{\text{cond.}} \sim |\Delta|^2$. In the deep BCS regime the energy required to create the ferron and the condensation energy become comparable and may even become lower, since the pairing gap decreases exponentially there. Therefore trying to induce local spin imbalance (the ferron) in the system, one may likely remove the pairing completely, placing the system in the normal phase. Consequently in the BCS limit the creation of a ferron may be practically difficult, as it will likely lead to the destruction of pairing correlations and creation of a normal system.

APPENDIX D: TDASLDA VS BdG DESCRIPTION OF THE FERRON

In this paper we have discussed the properties of ferronic excitation obtained within the TDASLDA approach, which was tuned to describe a spin-imbalanced UFG. The analysis indicates that the ferron's stability is due to the interplay between pairing and spin polarization and is therefore generic, not depending on the particular form of the functional. In

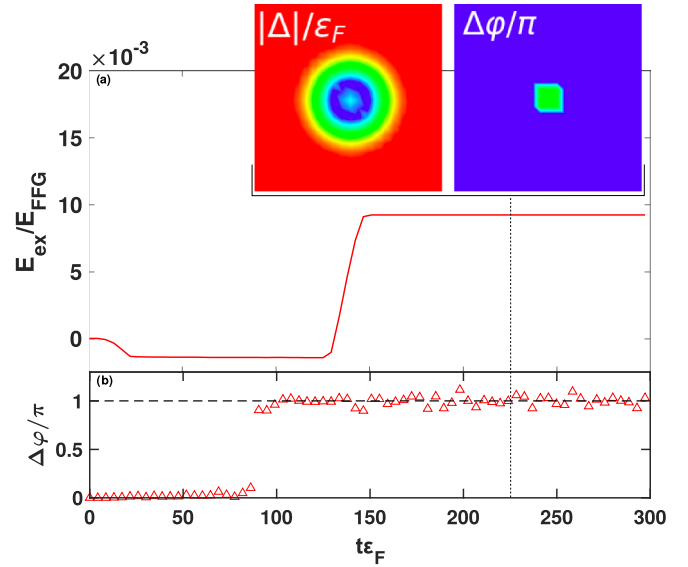


FIG. 15. Simulation demonstrating the ferron stability obtained within the BdG approach (see text for details). The total excitation energy $E_{\text{ex}} = E(t) - E(0)$ as a function of the time is shown together with the phase difference of the pairing field between the center of the ferron and the surrounding matter. The internal structure of the pairing field ($|\Delta|/\varepsilon_F$) and the phase pattern ($\Delta\varphi/\pi$) is also shown for selected time $t \approx 225 \varepsilon_F^{-1}$. The color coding is the same as in Fig. 9. For the full video see Supplemental Movie 15 [24].

order to illustrate this feature we have performed calculations within the Bogoliubov–de Gennes approach, where only a kinetic term and pairing term are present (no self-energy contribution). The pairing strength has been adjusted to produce a pairing gap corresponding to the unitary limit ($|\Delta|/\varepsilon_F \approx 0.5$). The results are shown in Fig. 15. The ferron has been created using the same technique as in the case of TDASLDA, i.e., by applying the external potential defined by Eq. (B1). The induced local spin polarization, after a certain time interval, generates a pairing phase difference inside the impurity [see Fig. 15(b)]. It is clearly shown that the structure of the ferron is qualitatively the same as obtained within the TDASLDA framework. Moreover, the stability of the created object is not affected. The difference between the BdG approach and the TDASLDA comes into play only in the process of ferron creation. Namely, the time needed to create the pairing phase flip inside the impurity turns out to be different in these approaches. Summarizing, the existence of a stable ferron is not sensitive to a particular form of the functional.

- [1] I. Bloch, J. Dalibard, and W. Zwerger, Many-body physics with ultracold gases, *Rev. Mod. Phys.* **80**, 885 (2008).
- [2] P. Fulde and R. A. Ferrel, Superconductivity in a strong spin-exchange field, *Phys. Rev.* **135**, A550 (1964).
- [3] A. I. Larkin and Y. N. Ovchinnikov, Nonuniform state of superconductors, *Zh. Eksp. Theor. Phys.* **47**, 1136 (1964) [*Sov. Phys. JETP* **20**, 762 (1965)].

- [4] G. Sarma, On the influence of a uniform exchange field on the spins of the conduction electrons in a superconductor, *J. Phys. Chem. Solids* **24**, 1029 (1963).
- [5] K. B. Gubbels, M. W. J. Romans, and H. T. C. Stoof, Sarma Phase in Trapped Unbalanced Fermi Gases, *Phys. Rev. Lett.* **97**, 210402 (2006).
- [6] C.-H. Pao, S.-T. Wu, and S.-K. Yip, Superfluid stability in the BEC-BCS crossover, *Phys. Rev. B* **73**, 132506 (2006).

- [7] H. Hu and X.-J. Liu, Mean-field phase diagrams of imbalanced Fermi gases near a Feshbach resonance, *Phys. Rev. A* **73**, 051603(R) (2006).
- [8] W. V. Liu and F. Wilczek, Interior Gap Superfluidity, *Phys. Rev. Lett.* **90**, 047002 (2003).
- [9] P. Castorina, M. Grasso, M. Oertel, M. Urban, and D. Zappalá, Nonstandard pairing in asymmetric trapped Fermi gases, *Phys. Rev. A* **72**, 025601 (2005).
- [10] J. Kinnunen, L. M. Jensen, and P. Törmä, Strongly Interacting Fermi Gases with Density Imbalance, *Phys. Rev. Lett.* **96**, 110403 (2006).
- [11] K. Machida, T. Mizushima, and M. Ichioka, Generic Phase Diagram of Fermion Superfluids with Population Imbalance, *Phys. Rev. Lett.* **97**, 120407 (2006).
- [12] B. Mukherjee, Z. Yan, P. B. Patel, Z. Hadzibabic, T. Yefsah, J. Struck, and M. W. Zwierlein, Homogeneous Atomic Fermi Gases, *Phys. Rev. Lett.* **118**, 123401 (2017).
- [13] A. I. Buzdin, Proximity effects in superconductor-ferromagnet heterostructures, *Rev. Mod. Phys.* **77**, 935 (2005).
- [14] K. Halterman and O. T. Valls, Layered ferromagnet-superconductor structures: The π state and proximity effects, *Phys. Rev. B* **69**, 014517 (2004).
- [15] G. Wlazłowski, K. Sekizawa, M. Marchwiany, and P. Magierski, Suppressed Solitonic Cascade in Spin-Imbalanced Superfluid Fermi Gas, *Phys. Rev. Lett.* **120**, 253002 (2018).
- [16] B. Van Schaeybroeck and A. Lazarides, Normal-Superfluid Interface Scattering for Polarized Fermion Gases, *Phys. Rev. Lett.* **98**, 170402 (2007).
- [17] M. M. Parish, D. A. Huse, Evaporative depolarization and spin-transport in a unitary trapped Fermi gas, *Phys. Rev. A* **80**, 063605 (2009).
- [18] A. Sommer, M. Ku, and M. W. Zwierlein, Spin transport in polaronic and superfluid Fermi gases, *New J. Phys.* **13**, 055009 (2011).
- [19] T. Enss and R. Haussmann, Quantum Mechanical Limitations to Spin Diffusion in the Unitary Fermi Gas, *Phys. Rev. Lett.* **109**, 195303 (2012).
- [20] A. Bulgac, P. Magierski, and M. M. Forbes, The unitary Fermi gas: From Monte Carlo to density functionals, in *BCS-BEC Crossover and the Unitary Fermi Gas. Lecture Notes in Physics*, edited by W. Zwerger (Springer, Heidelberg, 2012), Vol. 836, pp 305–373.
- [21] A. Bulgac and M. M. Forbes, Unitary Fermi Supersolid: The Larkin-Ovchinnikov Phase, *Phys. Rev. Lett.* **101**, 215301 (2008).
- [22] A. Bulgac, Y.-L. Luo, P. Magierski, K. J. Roche, and Y. Yu, Real-time dynamics of quantized vortices in a unitary Fermi superfluid, *Science* **332**, 1288 (2011).
- [23] A. Bulgac, M. M. Forbes, M. M. Kelley, K. J. Roche, and G. Wlazłowski, Quantized Superfluid Vortex Rings in the Unitary Fermi Gas, *Phys. Rev. Lett.* **112**, 025301 (2014).
- [24] See Supplemental Material at <http://link.aps.org/supplemental/10.1103/PhysRevA.100.033613> for videos visualizing dynamics of ferrons.
- [25] M. Lebrat, P. Grišins, D. Husmann, S. Häusler, L. Corman, T. Giamarchi, J.-P. Brantut, and T. Esslinger, Band and Correlated Insulators of Cold Fermions in a Mesoscopic Lattice, *Phys. Rev. X* **8**, 011053 (2018).
- [26] M. W. Zwierlein, Thermodynamics of strongly interacting Fermi gases, in *Proceedings of the International School of Physics “Enrico Fermi”*, Vol. 191 (ISO, Amsterdam, 2016), p. 143.